A NEW METHOD FOR MEASURING THE YIELD STRESS IN THIN LAYERS OF SEDIMENTING BLOOD

CHRISTOPHER L. MORRIS, CLARK M. SMITH II, AND PERRY L. BLACKSHEAR, JR.
Departments of Pediatrics and Mechanical Engineering, University of Minnesota, Minneapolis, Minnesota 55455

ABSTRACT A new method is presented to describe the low shear rate behavior of blood. We observed the response of a thin layer of sedimenting blood to a graded shear stress in a wedge-shaped chamber. The method allows quantitation of the degree of phase separation between red cells and plasma, and extracts the yield stress of the cell phase as a function of hematocrit. Our studies showed that the behavior of normal human blood underwent a transition from a solid-like gel to a Casson fluid. This transition began at the Casson predicted yield stress. The viscoelastic properties of blood were examined at shear stresses below the yield stress. The measured Young's elastic moduli were in good agreement with published data. The yield stress of blood showed a linear dependence on hematocrit up to 60%, and increased more rapidly at higher hematocrit.

INTRODUCTION

Blood is a non-Newtonian fluid with complex mechanical properties. Blood possesses viscoelastic properties that are governed by cell concentration, aggregation, deformation, and plasma viscosity (Chien, 1975). These properties vary with different shear rates. The viscous properties of blood dominate under most conditions, particularly high shear rates. However, under low shear conditions, elasticity becomes increasingly important. The non-Newtonian behavior of blood at low shear rates has been shown to be due to red cell membrane interactions (Cokelet, 1968). Thurston studied the elastic properties of normal blood. He found a strong dependence of the elastic modulus on frequency (Thurston, 1973) and hematocrit with approximately a cubed dependence on hematocrit (Thurston, 1972, 1978). Chien has extended these observations. He showed that at physiologic hematocrits, most of the elasticity of blood was dependent on the presence of plasma, suggesting that the elasticity of blood at low shear rates was due to cell rouleaux (Chien et al., 1975). The stress required to disaggregate the rouleaux of red cells in dextran 70 has been estimated to be ~0.25 dyn/cm^2 (Chien et al., 1977). The storage of energy in the elastic bonds of rouleaux suggests that blood could behave as a solid if examined under appropriate conditions.

There are many studies claiming a yield stress for blood (Merrill et al., 1963, 1965; Merrill, 1969; Cokelet, 1979; Copley et al., 1973; Huang et al., 1973); however, its existence remains controversial (Chien et al., 1966). Merrill and co-workers measured the yield stress of normal human blood and found values between 0.01 and 0.06 dyn/cm^2 at 40% hematocrit (Merrill et al., 1963; Merrill, 1969). The yield stress varied with the hematocrit cubed, similar to the dependence Thurston described for the elastic modulus of normal blood. Copley and King studied normal blood down to shear rates of 0.0009 s^{-1} and found evidence for a yield stress (Copley et al., 1973). The measurement of yield stress is complicated by the nature of blood and type of instrument used (Meiselman, 1980). Sedimentation, torque-time relations at low shear, edge effects, and wall exclusion effects are the major problems. All techniques of measuring yield stress are affected by the separation of blood into cell aggregates and plasma at low shear rates (see Cokelet, 1979). These difficulties are unfortunate because the yield stress of blood may be clinically important. Dormandy found elevated yield stress in patients with intermittent claudication (Dormandy et al., 1978). Humphreys showed a correlation between elevated yield stress and risk of deep vein thrombosis in postoperative patients (Humphreys et al.,1976). Radtke has developed a branched tube flow method of measuring yield stress that showed elevation in patients with diabetes mellitus (Radtke et al., 1984).

The primary aim of the present study is to present in detail a new method for measurement of the yield stress of blood which actually takes advantage of the tendency for cells to settle. Our method allows a thin layer of cells to settle on a flat horizontal surface and slump when the surface is set at an angle. As the cell layer is slumping, the yield stress and the hematocrit of the cell layer are measured. A broad range of hematocrits in the slumping cell layer were examined, thus establishing a yield stress-hematocrit relationship. The present study reports the range of yield stress as a function of hematocrit for normal

Address correspondence to Christopher L. Morris, M.D., Childrens Hospital Medical Center, Elland and Bethesda Avenues, Cincinnati, OH 45229.

whole blood anticoagulated with citrate-phosphate-dextrose. Analysis of the rheologic data employed a Casson model (casson vasa) that was solved for the case of a flowing film of blood with a one-dimensional velocity component. We also observed evidence of viscoelastic behavior of the cell layer. A secondary aim of the study is to provide preliminary data on the viscoelastic properties of blood as measured by our system.

METHODS

Theoretical Background

The response of a wedge-shaped sedimenting layer of blood cells to shear deformation was used to study the mechanical properties of blood at very low shear rates. A homogeneously mixed sample of blood was placed between two glass plates positioned so that the distance between the plates gradually decreased from 1,000 to 50 μm (Fig. 1 *a*). A sedimenting layer of cells formed with a discernible interface between the plasma and cell layer. Over a period of time dependent on the sedimenting characteristics of the cells and plasma, the hematocrit within the cell layer (H_p) increased to a maximum value, and sedimentation stopped. The height of the resultant cell pack was proportional to the distance between the plates.

The yield stress chamber was tilted along its long axis after the blood had formed a cell pack of variable thickness (Fig. 1 *a*). This was modeled as a flowing film with a one-dimensional velocity component. The force balance on the cell layer was given by:

$$\tau_{wc} - \tau_{cp} + \frac{H_0 T}{H_p}\left(\frac{dP}{dx} + \rho_p g \sin\theta\right) - (\rho_c - \rho_p) g H_0 T \sin\theta = 0, \quad (1)$$

where ρ_c equaled the density of the red cells, ρ_p was the plasma density, g the acceleration of gravity, H_0 the initial hematocrit of the blood injected into the chamber, H_p the hematocrit within the cell layer, τ_{wc} the shear stress at the wall-cell boundary, τ_{cp} the shear stress at the cell-plasma boundary, dP/dx the pressure gradient in the direction of cell flow, θ the angle the chamber was tilted, and T the vertical distance between the upper and lower plates. The thickness of the flowing film was given by H_0T/H_p. The quantity $-\tau_{cp} + (H_0T/H_p)\,(dP/dx - \rho_p g \sin\theta)$ was exactly zero if $\tau_{wc} \leq$ yield stress of the cell layer (τ_y), and was small compared with τ_{wc} for $\tau_{wc} > \tau_y$. Therefore to a good approximation throughout the chamber

$$\tau_{wc} = (\rho_c - \rho_p)\, g\, H_0\, T \sin\theta. \quad (2)$$

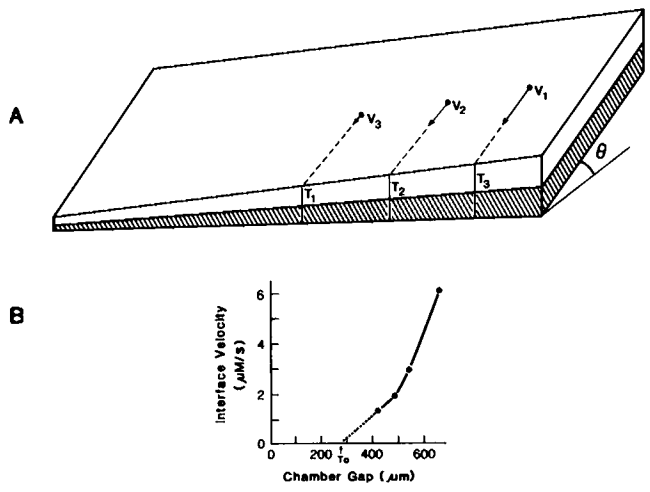

FIGURE 1 The yield stress chamber and wedge-shaped cell layer (hatched area) are illustrated in 1 *a*. The shear stress imposed on the cell pack by tilting at angle θ varied along the length of the chamber. The three gap widths (T_1, T_2, T_3) were associated with different cell layer surface velocities (V_1, V_2, V_3). Fig. 1 *b* shows the typical relationship between surface velocity and chamber gap width. The data were substituted into the Casson model which gave a mathematical extrapolation of the gap width, T_o, at which the shear stress equalled the yield stress of the cell pack.

In Appendix A the terms in the force balance of Eq. 1 were derived and the range of accuracy of Eq. 2 was analyzed. Although the shear stress at the cell-plasma interface is not zero the analysis in Appendix A shows that τ_{cp} is very small compared with the shear stress at the wall (τ_{wc}). The simplified analysis in Appendix B assumes Eq. 2 is valid, and does accurately predict the experimental data within the appropriate cell layer surface velocity range.

If the blood was initially distributed homogeneously throughout the chamber, and the cell pack hematocrit did not vary with T, the height of the cell pack was $T\,H_0/H_p$. The relationship between H_0 and T and the validity of the assumption was verified experimentally. Under these conditions, τ_{wc} was linearly dependent on T. The response of the cell pack to the applied shear stress was quantified by measuring the cell pack velocity at the cell layer surface as a function of the gap width as illustrated in Fig. 1 *b*. As the shear stress approached the yield stress of the cell pack, the interface velocity approached zero.

Analysis of the Stress-Response Relationship

We utilized a Casson model to evaluate the stress response:

$$\tau_c^{1/2} = \tau_y^{1/2} + (\eta_c\, dV_0/dy)^{1/2}, \quad (3)$$

where τ_c was the local shear stress of the cell layer, τ_y the yield stress of the cell layer, η_c the Casson coefficient of viscosity of the cell layer, and dV_c/dy the local shear rate. Eq. 3 was solved for the yield stress chamber geometry described above (see Appendix B); the cell pack interface velocity is given by

$$V_1 = \frac{\Delta\rho\, g \sin\theta\, H_0^2}{2\eta_c H_p}\, T^2\left[1 - \left(\frac{T_0}{T}\right)^{1/2}\right]^3\left[1 + \frac{1}{3}\left(\frac{T_0}{T}\right)^{1/2}\right], \quad (4)$$

where g, η_c, H_0, θ, and T are defined as before, H_p is the hematocrit within the cell layer at the time the cell layer velocity is measured, $\Delta\rho$ is $\rho_c - \rho_p$, V_1 is the velocity of the cell layer at the cell-plasma interface, and T_0 the gap width at which the Casson model predicts the wall shear stress to equal the yield stress. Gap width (T), cell layer surface velocity (V_1), cell layer hematocrit (H_p), and η_c were experimentally determined. Measurements at two adjacent points in the chamber ($T1$, $V1$, H_p1; $T2$, $V2$, H_p2) were substituted into Eq. 4; the ratio of the resulting two equations is:

$$\frac{V_1}{V_2} = \frac{H_{p2}}{H_{p1}}\left(\frac{T_1}{T_2}\right)^2\left[\frac{1 - (T_0/T_1)^{1/2}}{1 - (T_0/T_2)^{1/2}}\right]^3\left[\frac{1 + \frac{1}{3}(T_0/T_1)^{1/2}}{1 + \frac{1}{3}(T_0/T_2)^{1/2}}\right]. \quad (5)$$

T_0 was obtained numerically from Eq. 5, and inserted into Eq. 2 to obtain the Casson yield stress

$$\tau_y = (\rho_c - \rho_p)\, g\, H_0\, T_0 \sin\theta. \quad (6)$$

The analysis given in Appendix B assumed that H_p was constant throughout the cell pack, a condition satisfied over most of the area of the cell pack as presented in detail later. The analysis using Eq. 5 was limited to data where H_p varied by $\leq$3%.

EXPERIMENTAL METHODS

Blood was obtained from healthy adults in accordance with the committee on human subjects, and was drawn by antecubital venipuncture into

plastic syringes containing 3.8% trisodium citrate, pH 6.5 (93 mmol/liter sodium citrate, 70 mmol/liter citric acid, and 140 mmol/liter dextrose), at 9 vols blood to 1 vol anticoagulant. The blood was placed in plastic containers (Monoject, Div., Shorewood Medical, St. Louis, MO). Experiments were performed at room temperature and completed within 5 h of venipuncture. Whole blood was adjusted to hematocrit of 20–30% by dilution with autologous plasma. Citrated plasma was obtained from centrifugation of whole blood at 100 g for 10 min.

Plasma and Cell Density Measurement

Plasma density was measured by weighing a 200-μl pipette filled with fresh plasma on a model B6 Mettler balance (E.H. Sargent Co., Chicago, IL). The range of plasma density encountered in the study was 1.029–1.038 g/cm^3.

Red cell density was measured by weighing 200 μl of packed cells, subtracting the fraction of weight due to trapped plasma, and dividing by the hematocrit of the packed cells. Red cell density was given by

$$\rho_c = [W_c - W_p]/V_c, \tag{7}$$

where W_c was the weight (in milligrams) of 200 μl of blood, W_p was the weight of the plasma, and V_c was the portion of the 200 μl volume occupied by cells. After weighing, the 200-μl sample of blood was aspirated into three 70-μl capillary tubes, and hematocrit was determined in a model MB Micro hematocrit centrifuge (International Equipment Co., Damon Corp., Needham Heights, MA). The results of the three tubes were averaged. V_c (in microliters) = (hematocrit) $\times$ 200, W_p (in milligrams) = $[(200 - V_c) \times \rho_p]$. The resulting expression gave ρ_p in g/cm^3. For normal red cells the packing efficiency of the instrument was 0.99, and a value of 1.0 was assumed. However, for pathologic blood cells packing efficiency may be as low as 0.94. This requires the addition of a packing efficiency term (α_p) in Eq. 7 such that, V_c = 200 $\times$ (hematocrit) $\times$ α_p, or $\rho_c = (W_c - W_p)/V_c\,\alpha_p$. The range of cell density encountered with normal blood was 1.095–1.112 g/cm^3.

Yield Stress Chamber

Disposable yield stress chambers were constructed from two glass microscope slides 2.5 $\times$ 7 $\times$ 0.1 cm. The upper slide was a precleaned Clay Adam glass slide (Becton, Dickinson and Co., Oxnard, CA). The lower slide was an etched Dakin glass slide (Curtis Matheson Scientific, Minneapolis, MN) characterized by an irregular surface with 10-μm deep depressions. For consistent orientation the long axis will refer to the 7-cm dimension of the chamber and the short axis the 2.5-cm dimension. The middle of the long axis denotes a line parallel to the long axis 1.25 cm from either edge of the chamber. The chamber gap width is the vertical dimension of the chamber. The upper slide was gently etched with a diamond point pen along the middle of its long axis. This aided focusing on the upper plate when blood was in the chamber. An 18 or 20 gauge needle (Monoject) of ~1,000 or 700 μm diameter, respectively, was placed between the slides at one end, and a 50-μm foil shim was placed at the opposite end. The chamber was clamped gently and sealed with rapid drying epoxy (3M Scotch Brand, St. Paul, MN), avoiding obstruction of the outflow end of the needle. Only the narrow end of the chamber was left unsealed. The clamps and shim were removed after overnight drying. Excess epoxy was removed with a razor blade to allow the chamber to lie flush on a level surface. Each chamber was used once. The chamber was positioned vertically with the needle entry port at the bottom. Well-mixed whole blood was introduced into the chamber with a 3-cc non-luer lock plastic syringe. The chamber was filled over 10–15 s with 0.5–0.8 cc of blood. By taking at least 10 s to fill the chamber, we have not had a problem with red cell hemolysis. After loading the chamber the syringe is removed and the entry port immediately sealed.

Calculation of Cell Pack Hematocrit

The sealed chamber was placed on a level microscope stage. The distance between the upper plate and the cell-plasma interface (T_p) was measured visually with the microscope micrometer during sedimentation. The cell layer surface was easily identified as the cell pack image could only be resolved at the cell-plasma interface. The actual position was chosen by the best achievable focus of the cell layer and was reproducible within $\pm$2 mm. T_p was measured at multiple gap widths and after different times of sedimentation. Measurements were obtained midway across the short axis of the chamber and at least 0.5 cm away from the needle entry port. The total gap width at each position in the chamber was measured with the micrometer after the experiment was completed, and the cell pack removed from the chamber. Cell layer hematocrit was given by:

$$H_p = H_0\,[T/(T - T_p)], \tag{8}$$

where $T - T_p$ was the cell pack height at the gap width T. Microscope micrometer measurements were reproducible within $\pm$2 μm. The limiting factor in these measurements was the microscope optics. The micrometer accuracy was better than $\pm$0.1% of the total gap width. For the gap widths and cell pack heights encountered in our experiments the resultant variability in H_p was $\pm$1.5%.

The cell layer hematocrit was measured a minimum of four different sedimentation times at each of two to four gap widths. A cell layer hematocrit-sedimentation time curve was then constructed for each gap width (an example is shown in Fig. 4). The value of the cell layer hematocrit at the time at which the cell layer surface velocity was recorded was extrapolated from these curves.

The refractive index (RI) of the Clay Adams slides used in construction of the yield stress chamber was 1.52, and the RI of the plasma was 1.36. The difference in RI resulted in a distortion of the gap width measurement. The gap width measured with air in the chamber is the true gap. This was confirmed by placing a shim of known thickness between two microscope slides and measuring the resulting air gap. The same gap width was remeasured with a saline solution filling the gap. The gap width measured through saline was reduced by a factor equal to the ratio of the refractive index of air to saline. To obtain the true gap width the measurement in plasma should be multiplied by 1.36. This does not affect the cell layer hematocrit measurement since it is determined from a ratio that cancels out the correction factor. However, determination of the applied shear stress from Eq. 2 and the yield stress from Eqs. 3 and 4 must be corrected. Under these conditions the value of T_0 calculated from Eq. 5 is accurate and gives the correct yield stress when substituted into Eq. 6.

Cell Layer Surface Velocity Measurement

Cell layer surface velocity was measured from video recordings of the movement of the cell layer plasma interface soon after tilting the chamber. The cell pack was viewed from above through a 16$\times$ plane achromatic objective lens (NA = 0.35, free working distance ~4 mm) and 10$\times$ eyepiece of an upright zetopan microscope (Reichert, Vienna, Austria). A split prism delivered the image to a video camera (model HV-6256, Hitachi, Woodside, NY) connected directly to a video monitor (WV-5360, Panasonic, Secaucus, NJ) and video recorder (VO-2610, Sony, Tokyo, Japan). Before loading the yield stress chamber, external pen marks were made at four or five different gap widths along the midline of the chamber. T_p was measured at each of these gap widths at several different sedimentation times. Cell pack velocity was recorded after specified periods of sedimentation by tilting the microscope, with the microscope objective focused on the cell pack plasma interface and the VCR continuously recording. The cell pack interface velocity was recorded at each of the five marked positions starting with the greatest gap width and proceeding to the narrowest. Cell pack velocity was measured off the video monitor after completion of the experiment. The velocity at the initial position was measured 30 s after tilting to avoid motion artifact from the tilting and to standardize the measurement. Each subsequent position required 5–20 s observation to obtain sufficient movement on the monitor for measurement. Recording of the cell layer velocity was always completed within 120 s of tilting the chamber. The cell layer recordings were made along the middle of the short axis and at least 0.5 cm away from the needle entry port to avoid edge effects. During

the 2 min required to complete the recordings there was no significant change in the cell layer thickness at any point in the chamber except within 1–2 mm of the edges. Therefore edge effects were ignored, and the cell layer was assumed to be in steady state for the first 2 min of flow.

Wall Exclusion Equipment

Yield stress chambers were loaded with normal whole blood (H_0 = 39%), and allowed to completely sediment for 2 h. Total gap width (T), and cell pack thickness ($T - T_p$) were measured at ten gap widths varying from 100 to 1,200 μm in each of six yield stress chambers.

Cell Layer Hematocrit Experiments

The Casson analysis of the cell layer assumed that the cell layer is homogeneous with respect to hematocrit. In order to rule out changes in packing at the bottom of the cell layer due to gravity, we looked for evidence of variation in hematocrit in the vertical dimension of the cell layer. Yield stress chambers were scanned along the long axis in a spectrophotometer (model DU8; Beckman Instruments, Inc., Irvine, CA). The spectrophotometer had an attached slab scanner allowing the chambers to remain level while scanning. For these experiments, chambers were constructed from two clear Clay Adam microscope slides. All other aspects of chamber construction were as previously described. The chambers were allowed to sediment completely so that cell motion did not contribute to the optical density. The optical signal was maintained in the linear range for the instrument (0.100–0.900 OD units). When an OD of 0.900 was reached the spectrophotometer was rezeroed and the scan resumed, thereby generating a cumulative optical density. The wave length of the scan was chosen to limit the number of rezeroing procedures to 1. Cell pack hematocrit experiments were performed at a 600-nm wavelength (E_{600} = 0.80, Van Assendelft, 1970). The red cell pack was the only significant contributor to optical density. Scans of chambers filled with platelet-rich plasma at 600 nm showed no measurable difference in optical density between the thick and thin end of the chamber. We used an analysis of the spectrophotometric data that included the contributions of absorbance and scattering to the optical density of the cell layer (see Appendix C). The spectrophotometric data provided an assessment of the average cell layer hematocrit.

Cell Pack Elastic Modulus Experiment

The elastic properties of cell layers subjected to stresses below their yield stress were studied. Chambers were spectrophotometrically scanned across the short axis at one particular gap width. The chambers were scanned while level to obtain a baseline reading, and then rescanned with the chamber tilted. Tilting the chamber caused a slight elongation of the light path through the cell pack; however, this effect was equal at all points where the cell pack height was equal. Movement of the cell pack upon tilting caused the cell pack height to vary along the short axis of the chamber, and was detected as a deviation from the baseline scan. These studies were performed at 600 nm after complete sedimentation.

Statistics

Linear regression analysis was performed on the cell layer hematocrit data using a multiple regression interactive computer program developed by Weisberg (1980). By plotting the residuals of the linear regressions, it was possible to assess linearity through the full range of gap widths and detect any deviation from a linear function. The statistical significance of differences between individual linear regressions were determined by fitting the data to four separate discriminant models: intercept and slope different; different intercept but same slope; same intercept but different slope; same intercept and slope. The resulting sum of squares, residuals, F ratio, and coefficient of determination (R^2) was used to assess the validity of the models, and P values were determined from the ratio.

RESULTS

Several assumptions were made in solving the Casson equation and developing the force balance (Eqs. 4 and 2). Experiments were performed to establish the conditions under which the assumptions were accurate. These results will be presented first.

Wall Exclusion Studies

The force balance assumed that the initial hematocrit of the blood (H_0) was the same at all gap widths. However, wall exclusion effects may become significant at narrow gap widths. A yield stress chamber was filled with whole blood at 39% hematocrit and allowed to sediment completely. The cell layer thickness and gap width were measured at multiple gaps varying between 100 and 1,200 μm. The ratio of the cell layer thickness to the corresponding chamber gap width was constant for gap widths $\geq$800 μm. This ratio was then multiplied by the gap width for gaps <800 μm that gave the expected cell layer thickness at the narrower gaps. The observed divided by the expected cell pack height was expressed as the percent initial hematocrit, and was plotted as a function of the total gap width (Fig. 2). In 1929 Fahraeus described a phenomenon in which the hematocrit of blood flowing in narrow glass tubes was reduced compared with the hematocrit of blood entering the tube (Fahraeus, 1929). The degree of hematocrit reduction was dependent on tube diameter. We noted an unanticipated reduction of hematocrit in the narrow portion of the yield stress chamber. The effect was apparent with both smooth and roughened base slides. As shown in Fig. 2 the gap width at which the observed cell layer thickness began to deviate from the expected value correlated closely to the Fahraeus effect for circular tubes. Despite the obvious difference in geometry, the magnitude of hematocrit reduction in the yield stress chamber and circular tubes was approximately equal at comparable values of chamber gap width and tube diameter. The data in Fig. 2 indicated a 5% decrement in H_0 at 300 μm gap width. All yield stress measurements were performed at chamber gap widths >325 μm.

Cell Layer Hematocrit Studies

H_p was assumed to be homogeneous in the vertical dimension of the cell layer. Interpretation of the cell layer surface velocity may be erroneous if there is a large variation between the top and bottom hematocrit of the cell layer. Fig. 3 *a* shows the relationship between OD due to cell layer absorbance at 600 nm, and cell pack height ($T - T_p$) after 1 h of sedimentation. The scattering component of the optical density was calculated as described in Appendix C. The scattering component was subtracted from the total OD and the residual OD was then plotted as a function of $T - T_p$. The linearity of the curve in Fig. 3 *a* therefore suggested that the average cell layer hematocrit was

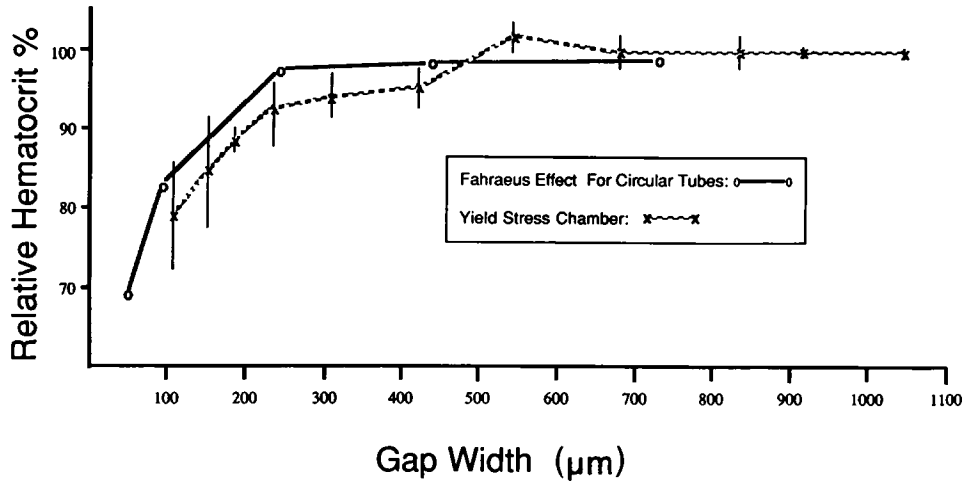

FIGURE 2 The hematocrit of the blood pumped into the yield stress chamber was plotted as a function of the local chamber gap width. The relative hematocrit was obtained from the ratio of observed to expected cell pack height, and was plotted against gap width (—x—). The expected cell pack height was calculated from the ratio of cell pack height to total gap for gap widths >800 μm. This ratio multiplied by the local gap width gave the expected cell layer thickness. The data of Fahraeus was plotted for comparison (—O—). The x-axis refers to tube diameter for the Fahraeus data. There was a rapid fall in hematocrit as the chamber gap width fell below 300 μm, similar to the Fahraeus effect in circular tubes.

constant as the cell pack height increased from 45 to 180 μm. The microscope optics made measurements of cell packs thinner than 45 μm difficult because of the variability in choosing a focal plane (±2 μm) became >10% of the total measurement.

In Fig. 3 *b* the data were plotted to look more sensitively for changes in the cell layer hematocrit. The rate of increase in OD 600 divided by the difference in cell layer height between two closely spaced points in the chamber was plotted against the average cell layer height of the two points. This essentially plotted the slope of the curve in 3 *a* against cell layer height. The scattering component of the

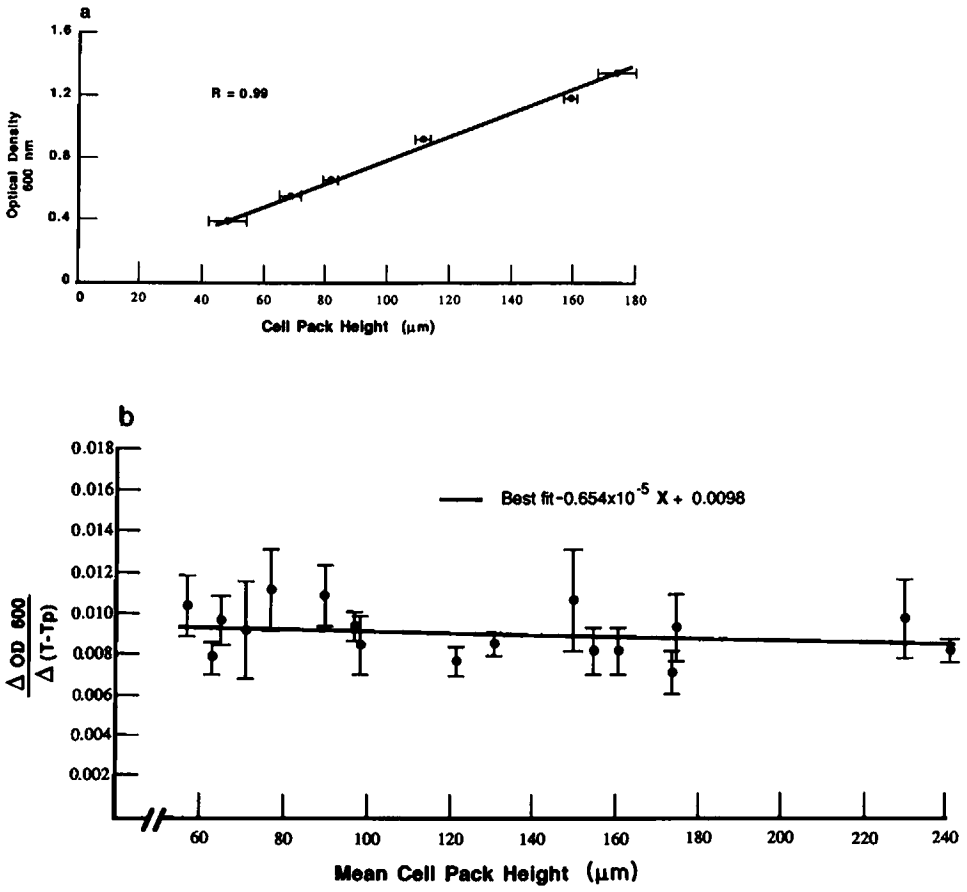

FIGURE 3 The relationship between optical density at 600 nm and cell pack height ($T - T_p$) across the long axis of the chamber is shown in Fig. 3 *a*. The component of optical density due to scatter was subtracted using the analysis in Appendix C. The data from four experiments fit the linear regression with R^2 values of 0.97, 0.98, 0.99, and 1.0. Fig. 3 *b* examines the relationship between cell pack hematocrit and height more closely. The increase in optical density divided by the change in cell pack height, $\Delta OD600/\Delta(T - T_p)$, between two closely spaced points in the chamber was plotted as a function of the average cell layer thickness of the two points. The scattering component of the optical density was subtracted. The data, when tested against the model $y = B_0$ + error (no slope), were not significantly different from a line of zero slope $P > 0.2$. The range bars represent standard error of the mean. The data are based on four experiments. The linear regression of the data resulted in a line defined by $Y = -0.654 \times 10^{-5} (T - T_p) + 0.0098$. Closely spaced points in the chamber were defined as a cell pack height difference <35 μm.

OD was subtracted before the calculation of the $\Delta OD/\Delta(T - T_p)$ ratio. The linear regression resulting from the data had a very slight negative slope, suggesting an unanticipated decrease in cell packing density as the cell layer thickened. However, when the regression line was tested against a zero slope model (Y = intercept ± error) they were statistically indistinguishable ($P > 0.2$). The results indicate that there was no significant variation in the average cell layer hematocrit as the cell layer increased in thickness between 50 and 240 μm. The fact that the average cell layer hematocrit remained constant for different layer thicknesses supports our assumption that the hematocrit was constant in the vertical dimension for a given thickness. The possibility that gravity might pack the cells tighter at the bottom of a thick layer than at the top can be ruled out because such tighter packing would result in an increase in the average layer hematocrit for thicker layers. It is conceivable that compensating differences in hematocrit might occur in different layers of the cell pack, but it is difficult to imagine what might cause such compensating variations, and the possibility appears unlikely. When solved under the assumption of a homogeneous cell layer hematocrit, the Casson model accurately predicted the experimentally measured cell layer velocities, as shown below. Thus the assumption that hematocrit is constant over the thickness of the cell pack is consistent with all of our experimental observations, and provides the most plausible explanation of our experimental results.

Fig. 4 demonstrates the increase in H_p with the time of sedimentation at three different gap widths. The maximal H_p was achieved more rapidly at lower gap widths. The H_p distribution equalized throughout the chamber within 30 min. For sedimentation times <30 min, H_p varied across the chamber. When the H_p variation between data points was larger than 3%, a yield stress was determined by comparing two positions in the chamber that were closer together, with corresponding smaller differences in H_p. Thus, even for low hematocrit cell packs that were rapidly sedimenting, it was possible to determine a yield stress.

Influence of Plasma Flow on the Cell Layer Surface Velocity

The yield stress chamber is a closed system, therefore the flowing cell layer must displace an equal volume of plasma.

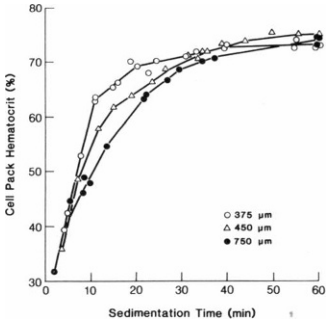

FIGURE 4 The increase in cell pack hematocrit (H_p) with time of sedimentation is shown at three different gap widths. H_p increased more rapidly at the smaller gap widths, and achieved uniformity across the chamber after 25 min of sedimentation. The initial hematocrit of the blood sample was 25%.

This results in a net flow of plasma opposite to the flow of cells, producing the force balance of Eq. 1. The plasma flow exerts a drag on the cell layer at the cell-plasma interface, τ_{cp}, and alters the pressure gradient in the chamber. The force balance equation assumes that the local velocity component in the cell and plasma phases are one dimensional in the direction of tilt. Experimental observations of the cell layer did not show evidence for flow normal to the direction of tilt except under conditions in which the cell layer surface velocity was extremely high (50–100 μm/s). Observations of the plasma phase were made by moving the focal plane of the microscope to observe the motion of platelets. These studies showed the platelets move in the opposite direction of the cell phase parallel to the axis of tilt.

We analyzed the shear stress profile across the chamber using a Casson model for the cell phase and a Newtonian one for the plasma phase, and assuming one-dimensional laminar flow in each phase. Fig. 5 displays a model of the analysis. The shear stress at the interface resulting from the plasma flow was calculated by matching the cell and plasma velocities at the interface, and the volume flows ($-Q_p = Q_c$). The deviation from the non–plasma flow assumption [$\tau_{wc} = (\rho_c - \rho_p)\, g\, H_0\, T \sin\theta$] was found to be small as long as the cell layer surface velocity was <20 μm/s. The analysis is detailed in Appendix A.

Viscoelastic Properties of the Cell Layer

Fig. 6 shows the variation of cell pack interface velocity as a function of time after tilting and again after releveling the chamber. These experiments were performed to observe the transition from elastic deformation of the cell pack to viscous flow. The chambers were carefully tilted to minimize motion artifact and allow measurement of the cell layer velocity within the first few seconds of tilting or releveling. The behavior of the cell pack interface was observed at four gap widths. The shear stress at one gap width was below the yield stress (Fig. 6 *a*) and the other three were at shear stresses progressively greater than the yield stress (Fig. 6, *b–d*). Below the yield stress the cell pack interface moved with a small initial velocity that rapidly decayed toward zero after tilting the chamber (Fig. 6 *a*). Stress greater than the yield stress resulted in larger initial interface velocities that decayed to a measurable plateau velocity. Initial and plateau velocities increased stepwise as the shear stress exceeded the yield stress by greater margins (Fig. 6, *b–d*). Releveling of the chamber after 90–120 s of forward flow resulted in immediate flow of the cell layer in the reverse direction which rapidly decayed to zero. The magnitude of the initial velocity was identical for reverse and forward interface flow, and the length of time for the forward flow to plateau and the reverse flow to decay to zero was equal.

The displacement of the cell pack at shear stresses under the experimentally determined yield stress was evaluated more closely. A chamber with fully sedimented blood was

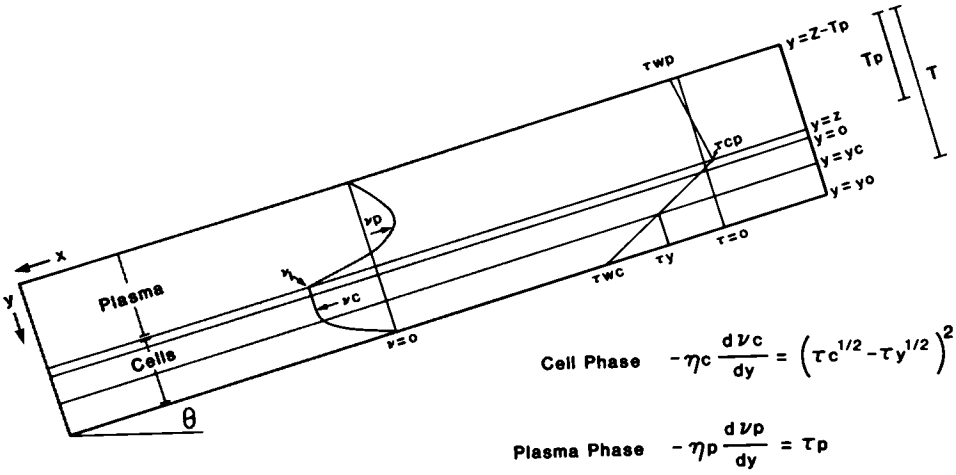

FIGURE 5 The velocity and shear stress profile of the cell layer and counter plasma flow in the tilted yield stress chamber is shown. The plasma layer flowing in the opposite direction of the cell pack exerts resistance to the cell layer flow at both the cell-plasma interface and the cell-wall boundary. τ_{wc}, τ_{wp}, and τ_y are the shear stress at the cell-wall, plasma-wall interfaces and the yield stress, respectively. z and y_o are the y-coordinates at the cell-plasma and cell-wall interfaces, and y_c is where the cell layer shear stress equals the yield stress.

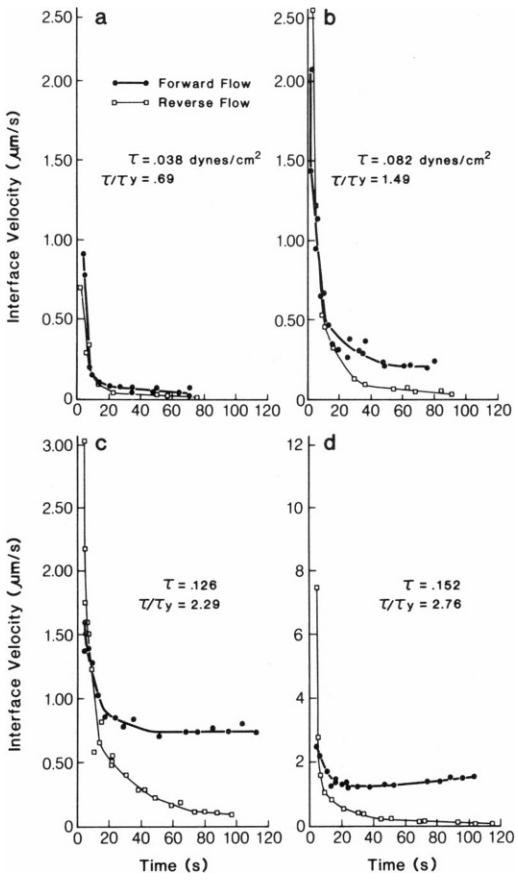

FIGURE 6 The velocity of the cell layer in response to different applied shear stresses is shown as a function of time after tilting (forward flow, ●) and after releveling (reverse flow, □). An applied shear stress less than the experimentally determined yield stress is shown in *a*, and stresses progressively greater than the yield stress are shown in *b*, *c*, and *d*. The cell layer surface underwent an initial displacement after which its velocity decayed to zero when the applied stress was under the yield stress. When the applied shear was greater than the yield stress the cell layer demonstrated a plateau velocity 20–40 s after tilting. This velocity increased as the applied shear exceeded the yield stress. The experiments were performed on blood from one donor at H_p 67% (τ_y = 0.055 dyn/cm²). Three other experiments showed similar results.

tilted and spectrophotometrically scanned across the short axis at a gap width and tilt angle corresponding to a shear force below the yield stress. The cell layer underwent a rapid displacement that was completely reversible, as illustrated in Fig. 7. The displacement of the cell pack increased with the application of greater shear stress (Fig. 7, *b* and *c*), but did not change over 5 min of maintenance of the stress (Fig. 7, *c* and *d*). The cell pack rapidly returned to the original configuration after releveling of the chamber and removal of the shear stress (Fig. 7 *e*). The elastic behavior of the cell pack was also studied by direct microscopic observation during unloading of the shear stress. The magnitude of the displacement of the cell pack surface in the plane of the interface (δ) was measured during releveling of the chamber and compared with the cell pack height ($T - T_p$). The displacement was small at shear stresses under the yield stress; $\delta/(T - T_p)$ remained <5% and allowed the use of Hookes Law, $E = \tau/[\delta/(T - T_p)]$ to calculate the shear elastic modulus (E) of the cell layer (Fung, 1984). During four experiments in which H_p varied from 68 to 75% the elastic modulus ranged from 1.1 to 2.2 dyn/cm². It was difficult to compare these results directly to elastic modulus data obtained by oscillatory

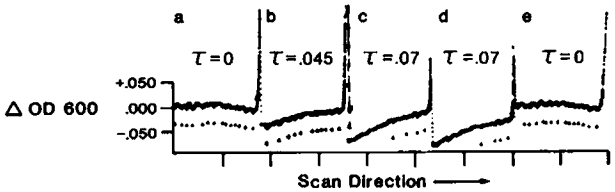

FIGURE 7 Several spectrophotometric scans across the short axis of the chamber show the elastic behavior of the cell layer during the application of shear stresses less than the yield stress. The left axis refers to the change in optical density at 600 nm in absorbance units standardized against the optical density of the level cell pack. The scan direction proceeds from the top to the bottom of the chamber. The magnitude of the stress was changed by altering the angle of tilt from 0 to 12 degrees; gap width was 310 μm and τ_y = .075 dyn/cm². Fig. 7 *a* shows a scan of the level chamber; *b*, after 2 min of τ_{wc} = 0.045; *c*, after 2 min of τ_{wc} = 0.7; *d*, after 5 min of τ_{wc} = 0.7 dyn/cm²; *e*, chamber releveled. An increment of 0.05 OD600 represented a 2% change in cell pack height.

viscometry as the frequency of oscillation appears to influence the result. However if one calculates the elastic modulus from the data of Chien or Drasler for frequency of 1 Hz and hematocrit of 80% their results are in reasonable agreement with our observations: ~0.8 dyn/cm^2 at 80% hematocrit (Chien) vs. 1 dyn/cm^2 at 75% hematocrit (Chien, et al., 1975; Drasler, 1984).

Comparison of Experimental Results with the Casson Model

In Fig. 8 the observed stress response of the cell pack interface is compared with the Casson predicted behavior for 10, 20, and 60 min sedimentation (H_p = 53, 65, and 72%, respectively). The Casson predicted curve was based on extrapolation from the data point with the greatest shear stress. These studies showed excellent agreement of the experimental data with the Casson model at shear stress >1.5 times the Casson extrapolated yield stress corresponding to interface velocities >0.5–3 μm/s. The Casson model accurately predicted the relationship between applied shear stress and interface velocity even for cell packs with H_p up to 75%. A progressive deviation from Casson behavior was apparent on approaching the yield stress. The departure was not due to slippage of the cell pack over the glass base slide. Microscopic observation of the superior edge of the etched base slide did not detect any cell-free areas despite tilting the chamber at 45° angle for up to 60 min. As can be seen in Fig. 5 the velocity profile of the cell pack was curved, therefore the shear rate was not constant. A representative cell layer shear rate was calculated by dividing the cell layer surface velocity by cell layer thickness minus *yc*, the thickness of the plug flow region. Deviation from Casson behavior was noted at shear rates of $5 \times 10^{-3}\,s^{-1}$, $<5 \times 10^{-3}\,s^{-1}$, and $1 \times 10^{-2}\,s^{-1}$ for the 10-, 20-, and 60-min sedimentation times, respectively. Huang et al. (1973) noted a transition between liquid and solid behavior of blood at nearly identical shear rates using a Weissenberg rheogoniometer.

Yield Stress of Normal Blood

The Casson-predicted yield stress of blood from nine healthy adult donors is shown as a function of cell pack hematocrit in Fig. 9. Each donor was studied on one to four occasions with two to five yield stress chambers per study. The data shows an apparently linear increase in yield stress for H_p between 45 and 65%, after which yield stress increased more steeply.

DISCUSSION

We have developed a method that allows accurate determination of the yield stress of normal blood at hematocrits between 40 and 80%. The stress response of the cell layer at

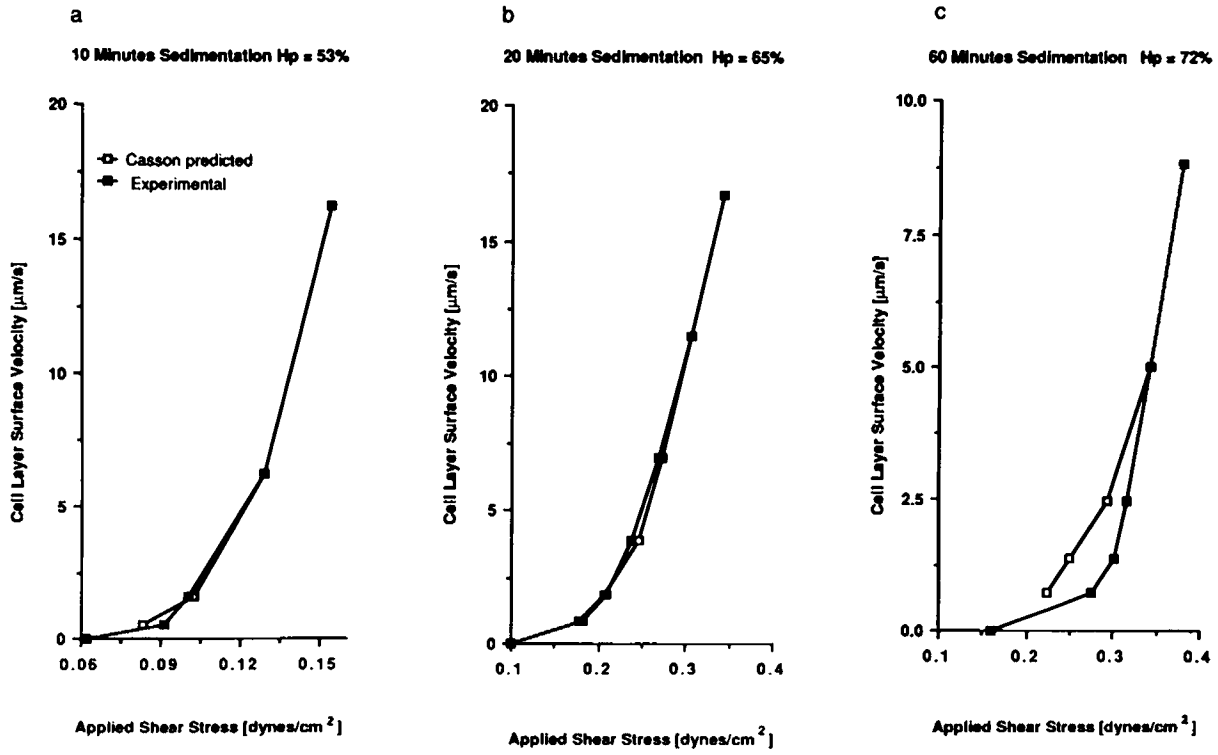

FIGURE 8 The experimentally measured (■) stress response of the cell pack is contrasted with the Casson predicted behavior (□) after differing sedimentation times. The cell layer surface velocity is plotted against applied shear stress. Surface velocity refers to the plateau velocity measured 30–90 s after tilting the chamber. The Casson fit (□) was constructed by calculating the value of T_0 from the high shear stress data point using Eq. 5 (see text). The calculated T_0 was then used to predict the shear stress at each subsequent gap width that would give the experimentally measured surface velocity.

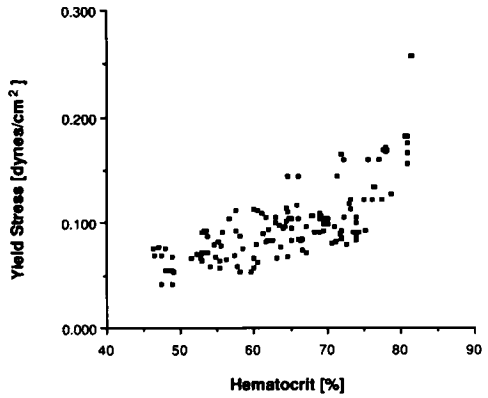

FIGURE 9 The yield stress of normal blood is shown as a function of cell pack hematocrit. The data are based on 45 yield stress chamber experiments performed on 19 blood samples from nine healthy adult donors ages 25–38.

shear rates above 0.5–1 $\times 10^{-2}\,s^{-1}$ was correctly predicted by a Casson model. At shear rates below this range the blood behaved as a viscoelastic fluid with a very large viscous coefficient. Our system detected the transition from Casson fluid to viscoelastic solid and provided data on the viscoelastic properties of the blood cell layer.

In studies in which cell sedimentation limited the low shear rate measurements, the presence of a Casson region was dependent on hematocrit. The shear rate threshold for the Casson region decreased below the range of shear rates encountered in these studies as hematocrit increased. Normal blood below 40% hematocrit behaved as a Casson fluid up to shear rates of 20 s^{-1} above which there was a gradual transition to Newtonian behavior (Merrill and Pelletier, 1967). The Casson region appeared to shift to lower shear rates and eventually vanish as the hematocrit increased. Cokelet, using the data of Brooks et al. (1970), showed that the plot of (shear stress)$^{1/2}$ vs. (shear rate)$^{1/2}$ became linear at lower values of shear rate as hematocrit increased (Cokelet, 1979). Brooks has obtained data for hematocrits as high was 67.4% at shear rates down to 0.2 s^{-1}. Within this range of shear rates, a Casson region did appear to exist for hematocrits <47% (Cokelet, 1979). The shear rates encountered in the yield stress chamber were determined from the cell layer surface velocity. The maximum velocities used in our study were 20 μm/s in order to avoid plasma drag effects. The velocity gradient of the cell layer (dV_c/dy) was not constant, however a representative value of the shear rate was obtained by dividing $V_c/(T - T_p - yc)$ (see Fig. 5). For V_c = 19.4–23.5 μm/s typical values of $(T - T_p - yc)$ were 250–275 μm. This resulted in a representative shear rate of 8–8.5 $\times 10^{-2}\,s^{-1}$. For these low shear rates there is no data available from other sources to compare the present results with since the literature data have a vanishing Casson region at hematocrit >47%, presumably because of cell sedimentation. We found the Casson model accurately predicted the behavior of sedimented cell layers for hematocrits between 45 and 80% as long as the applied shear stress was at least 1.5 times the Casson predicted yield stress.

The yield stress of blood shows an apparently linear rate of increase for cell layer hematocrits between 45 and 60%. Above a hematocrit of 60–65% there is an accelerating rate of increase in the yield stress. In contrast, Merrill reported that the yield stress of normal blood increased as the third power of hematocrit between 10 and 40%, but the data showed a fall in the rate of increase above 40% hematocrit (Merrill et al., 1963). Our data show a range of yield stress between 0.04 and 0.070 dyn/cm^2 at 45% hematocrit, which is very close to the results of Merrill. This suggests the possibility that sedimentation effects at low hematocrit may have artifically enhanced the dependence of yield stress on hematocrit in Merrill's study. This would explain why our data are in good agreement at hematocrits of 45% where sedimentation effects would be considerably less. Alternatively there may be a change in the way rouleaux are linked leading to a different dependence of yield stress on hematocrit above and below 40%.

The dominant behavior of the cell layer changed from a Casson fluid to a viscoelastic solid at shear stresses near 1.5–2.0 times the yield stress, corresponding to shear rates of 0.5–1.0 $\times 10^{-2}\,s^{-1}$. The results agree with observations of several other investigators. Copley reported data for normal blood sheared between 10^{-3} and $10^{+3}\,s^{-1}$ using a modified Weissenberg rheogoniometer (Copley et al., 1973). His data showed three distinct regions. The region above 50 s^{-1} was Newtonian. At shear rates <50 s^{-1} there was a gradual transition to a Casson region of behavior. In the very low shear rate region (10^{-2}–$10^{-3}\,s^{-1}$) normal blood ceased to behave according to the Casson equation. Huang interpreted the behavior as representing a viscoelastic cell phase slipping over a plasma boundary (Huang et al., 1973).

These results suggest that blood behaves as a viscoelastic solid when examined under sufficiently small stress, a finding consistent with other investigators' work using standard methods (Thurston, 1972, 1973, 1978; Chien et al., 1975). Our data offer further confirmation of the existence of a transition region between predominantly viscous behavior described by the Casson equation and predominantly elastic behavior described by a viscoelastic model. The transition began to occur at shear stresses 1.5–2 times the Casson predicted yield stress and was completed at the yield stress point. This transition region may be of physiologic significance in conditions associated with sluggish blood flow, as the transition of pressure into flow may become much less favorable at a shear stress below twice the yield stress.

Applying a shear stress less than the yield stress resulted in elastic displacement of the cell pack with a rapid decay in the cell layer surface velocity toward zero. Deformation due to stress applied for short times was completely reversible, and the elastic modulus calculated from the data was in good agreement with other published values.

Use of the theoretical analysis to determine yield stress required an accurate determination of H_p. We have shown that H_p became uniform along the long axis of the chamber after 30 min of sedimentation. Additionally, for sedimentation times >60 min we showed that the average cell layer hematocrit did not change as the cell layer varied in thickness from 50 to 240 μm, suggesting that H_p was uniform in the vertical dimension of the cell pack. Brooks demonstrated that fully sedimented normal erythrocytes suspended in saline could support a column 420 μm high before the cells deformed (Brooks et al., 1970). He found that if the hematocrit of the column were >60%, the cells would deform. However, in a plasma system rouleaux formation would greatly increase this hematocrit estimate. The force acting to deform the red cell is proportional to $(\rho_c - \rho_{susp})$, which is ~30% smaller for plasma compared with saline suspensions. Therefore, the cell layer thickness at which demonstrable cell deformation would occur would be >500 μm for a plasma system. These findings further support the contention that for long sedimentation times H_p has minimal variation in the vertical dimension for thin cell layers.

When sedimentation time was short, we compared data from positions closer in the horizontal plane of the chamber to assure that variation of H_p between data points was small. However, we were left with uncertainty concerning the uniformity of H_p in the vertical direction for short sedimentation times. Whelan studied the hematocrits of normal blood in large diameter, 20-cm-tall tubes at various hematocrits and sedimentation times by sampling the hematocrit at various depths below the cell pack plasma interface (Whelan et al., 1971). For long sedimentation time, there was very slight variation, 2–4% decrease in hematocrit of top compared with bottom fraction, over the 10-cm height of the cell pack. For the shortest sedimentation time (1 h), the variation between top and bottom fraction was 19% (35% top vs. 54% bottom); however, this difference was spread over 19 cm, and the variation over the top centimeter of the cell pack was only 4%. The maximum cell layer thickness in our study was 0.05 cm. It seems reasonable that the variation in hematocrit of extremely thin layers of red cells would be less than that seen in Whelan's system. It is also likely that a major decrease of hematocrit in the upper cell layer would result in an increased sedimentation velocity of the top relative to bottom cell layer, and for such thin cell layers this would tend to restrict the growth of any large differences in hematocrit. Considering the excellent fit of our experimental data to the Casson model, it may be that by the time the cell layer has achieved a 40–50% hematocrit the vertical variation in H_p has become negligible.

The yield stress chamber provided a means of quantitatively assessing the properties of erythrocyte suspensions at very low shear rates. Our studies were performed at high, mostly nonphysiologic hematocrits. However, this facilitated quantitative measurement of the yield stress which reflected the adhesiveness of individual red cells. The normal range of red cell yield stress as a function of hematocrit was determined to allow comparison of the adhesive characteristics of pathological red cells to normal erythrocytes. Examination of high hematocrit suspensions by our method enabled us to assess the accuracy of the Casson model at shear rates and hematocrits not previously studied. Lastly, we were able to measure the shear elastic modulus of the cell layer and show that our results agree with values obtained from standard viscometry methods.

APPENDIX A

The shear stress and velocity profiles across the short axis of the yield stress chamber are illustrated in Fig. 5. We will analytically solve the velocity profile and volumetric flow of the cell and plasma phase. The wall shear stress of the cell layer (τ_{wc}) will be calculated taking into account the plasma flow. This value of τ_{wc} will be compared with the ideal value: $\tau_{wc} = \Delta\rho\, g\, H_0 T \sin\theta$, which ignores plasma flow effects. Assuming one-dimensional flow in the direction of tilt continuity requires that the volume flows in the plasma and cell phase be equal: $\{[Q_p] = -[Q_c]\}$. To evaluate the influence of plasma flow we will use the experimentally determined value of the cell layer surface velocity (V_l), continuity, and equal velocities at the cell-plasma interface ($V_p = V_c = V_l$ at $y = z$).

$$-\int_{z-T_p}^{z} V_p\, dy = \int_{z}^{y_o} V_c\, dy. \tag{A1}$$

The velocity of the plasma (V_p) is integrated over the width of the plasma phase (T_p), and the cell pack velocity (V_c) is integrated over the cell layer thickness $y_o - z$, (see Fig. 5). Integrating the Casson equation (Eq. B1 in Appendix B) with the condition $\tau_c = (y/y_o)\,\tau_{wc}$, where τ_c is the local shear stress in the cell phase and $V_c = 0$ at $y = y_o$ we have:

$$V_c = \frac{\tau_{wc}\, y_o}{2\,\eta_c}\left[1 - \left(\frac{y}{y_o}\right)^2 + \frac{8}{3}\left(\frac{y_c^{1/2}\, y^{3/2}}{y_o^2}\right) - \frac{8}{3}\left(\frac{y_c}{y_o}\right)^{1/2} - 2\left(\frac{y_c\, y}{y_o^2}\right) + 2\left(\frac{y_c}{y_o}\right)\right]. \tag{A2}$$

y_o is the cell wall interface, and y_c the position where τ_c equals the yield stress τ_y. At $y = y_c$, $V = V_{max}$,

$$V_c = \frac{\tau_{wc}\, y_o}{2\,\eta_c}\left[1 - \frac{1}{3}\left(\frac{y_c}{y_o}\right)^2 + 2\left(\frac{y_c}{y_o}\right) - \frac{8}{3}\left(\frac{y_c}{y_o}\right)^{1/2}\right]. \tag{A3}$$

The volume flow of the cell phase is given by $\delta V_{max} + \int_{y_c}^{y_o} V_c\, dy$, where δ is the thickness of the plug flow region and is given by $(y_c - z)$. Note that z is the distance between the cell-plasma interface where $\tau_c = \tau_{cp}$, and $y = 0$ where $\tau_c = 0$. If $|z| < y_c$ then $|\tau_{cp}| < \tau_y$ and the plug flow region includes the cell-plasma interface. The volume flow of the cell phase (Q_c) is given by:

$$Q_c = \delta V_l + \frac{\tau_{wc}\, y_o^2}{2\,\eta_c}\left[\frac{2}{3} - \frac{8}{5}\left(\frac{y_c}{y_o}\right)^{1/2} + \frac{8}{3}\left(\frac{y_c}{y_o}\right)^{3/2} - 2\left(\frac{y_c}{y_o}\right)^2 + \frac{4}{15}\left(\frac{y_c}{y_o}\right)^3\right]. \tag{A4}$$

For the plasma phase we can write a force balance for gravity driven flow:

$$\frac{d\tau_p}{dy} = -\frac{dP}{dx} + \rho_p g \sin\theta = K, \tag{A5}$$

where K is the slope of the plasma phase shear stress profile and is given

by:

$$K = (\tau_{cp} - \tau_{wp})/T_p. \quad \text{(A6)}$$

τ_{cp} is the shear stress at the cell-plasma interface, and τ_{wp} is the shear stress at the plasma-wall interface. At $y = y_o - T$, $\tau_p = \tau_{wp}$, then integrating Eq. A5 with these boundry conditions we have:

$$\tau_p = K(y + T - y_o) + \tau_{wp} \quad \text{and} \quad \tau_p = -\eta_c \, dV_p/dy. \quad \text{(A7)}$$

Substituting and integrating with boundary conditions $y = y_o - T$, $V_p = 0$, we have

$$V_p = -\frac{K}{2\eta_p}(y + T - y_o) - \frac{\tau_{wp}}{\eta_p}(y + T - y_o). \quad \text{(A8)}$$

At $y = z$, $V_p = V_l$ (note: $z = -[T - T_p - y_o]$), and substitution for K with Eq. A6 gives:

$$V_l = -\frac{T_p \tau_{wp}}{2\eta_p}\left(\frac{\tau_{cp}}{\tau_{wp}} + 1\right). \quad \text{(A9)}$$

The plasma volume flow is obtained by integrating Eq. A8 after substituting for K from Eq. A6. From Eqs. A5 and A6 we can substitute for $-dP/dx + \rho_p g \sin\theta$, giving

$$\int_{y_o - T}^{z} V_p \, dy = -\frac{T_p^2}{2\eta_p}\tau_{wp}\left[\frac{2}{3} + \frac{\tau_{cp}}{2\tau_{wp}}\right] = Q_p. \quad \text{(A10)}$$

Note that:

$$\tau_{cp} = (z/y_o)\tau_{wc} \quad \text{(A11)}$$

$$\delta = (T - T_p + y_c - y_o) \quad \text{(A12)}$$

$$y_c = \tau_y/[(\rho_c - \rho_p)H_p \, g \sin\theta]. \quad \text{(A13)}$$

A force balance across the width of the chamber gives

$$\tau_{wp} - \tau_{wc} - \frac{dP}{dx}T + \rho_p g \sin\theta T(1 - H_0) + \rho_c g \sin\theta H_0 T = 0. \quad \text{(A14)}$$

From Eqs. A5 and A6 we can substitute for $-dp/dx + \rho_p g \sin\theta$ in Eq. A14, giving:

$$\tau_{wc} = \frac{\tau_{wp}(1 - T/T_p) + c}{(1 - zT/T_o y_o)}, \quad \text{(A15)}$$

where $c = (\rho_c - \rho_p)\, g \sin\theta \, TH_0$. We set Eq. A3 = Eq. A9 at the cell plasma interface ($V_c = V_p = V_l$ at $y = z$), and Eq. A4 = Eq. A10 ($Q_c = -Q_p$). Using Eqs. A11, A12, A15, and the experimental values for T, T_p, η_c, η_p, c, y_c, and V_l, we have two equations with τ_{wc} as a function of z. These two functions can be plotted, and their point of intersection gives the wall shear stress satisfying all four equations. Several examples are tabulated below using $\eta_c = 6$cp, $\eta_p = 1.2$cp.

V_l	H_p	$\tau_{wc}/(\tau_{wc}$ ideal)	τ_y	τ_{cp}	Z
$\mu m/s$	%	%		dyn/cm^2	μm
35.8	45.0	83.7	0.049	−0.0084	−21
19.4	46.5	89.5	0.052	−0.0059	−13
10.0	47.0	93.5	0.056	−0.0030	−6.7

The maximal deviation from ideal behavior due to the plasma drag is 10% at an interface velocity of 20 μm/s and H_p 46%. Our normal data in Fig. 9 utilized interface velocities <20 μm/s and $H_p > 44\%$, with most of the velocities between 1.5 and 10 μm/s. Note that the interface shear stress τ_{cp} is always much less than τ_y, and therefore the assumption of plug flow between y_c and the interface is valid.

APPENDIX B

We will derive the maximum cell pack velocity under the condition that the shear stress is zero at the cell plasma interface. The conditions under which this assumption is valid were defined in Appendix A. The Casson relation is given by:

$$\eta_c(dV_c/dy) = -(\tau_c^{1/2} - \tau_y^{1/2}), \quad \text{(B1)}$$

where η_c is the Casson viscosity coefficient, V_c the velocity of the cell phase, and τ_c, τ_y the shear stress in the cell phase and yield stress, respectively. The cell phase shear stress is also given by (see Fig. 5)

$$\tau_c = (y/y_o)\,\tau_{wc}, \quad \text{(B2)}$$

where τ_{wc} is the shear stress at the cell-wall boundary and y_o is the cell pack thickness. We will integrate from the cell wall boundary $y = y_o$ to y_c, where y_c in the point in the cell phase that $\tau_c = \tau_y$. At y_c, $V_c = V_{max}$, and at y_o, $V_c = 0$.

$$\eta_c V_{max} = -\left[\frac{\tau_{wc}}{2y_o}(y_c^2 - y_o^2) - \frac{4}{3}\left(\frac{\tau_y \tau_{wc}}{y_o}\right)^{1/2} \cdot (y_c^{3/2} - y_o^{3/2}) + \tau_y(y_c - y_o)\right]. \quad \text{(B3)}$$

From Eq. A2, $\tau_y = (y_c/y_o)\tau_{wc}$; and letting $y_o = (H_0/H_p)T$, $y_c = (H_0/H_p)T_o$, where T_o is the gap width at the yield stress point, we have

$$V_{max} = \frac{\tau_y H_0 T^2}{2\eta_c H_p T_o}\left[1 - \frac{1}{3}\left(\frac{T_o}{T}\right)^2 + 2\left(\frac{T_o}{T}\right) - \frac{8}{3}\left(\frac{T_o}{T}\right)^{1/2}\right]. \quad \text{(B4)}$$

From Fung, 1984, we have:

$$V_{max} = \frac{\tau_y H_0 T^2}{2\eta_c H_p T_o}\left[1 - \left(\frac{T_o}{T}\right)^{1/2}\right]^3\left[1 + \frac{1}{3}\left(\frac{T_o}{T}\right)^{1/2}\right]. \quad \text{(B5)}$$

For $|\tau_c| \le \tau_y$, $V_c = V_{max}$. If we assume that $|\tau_c|$ at the interface is less than τ_y, then $V_{max} = V_l$. This assumption is validated in Appendix A. Substitution of V_l for V_{max}, and $\Delta\rho g H_0 T_o \sin\theta$ for τ_y gives the solution for the cell plasma interface velocity:

$$V_l = \frac{\Delta\rho \, g \sin\theta H_0^2}{2\eta_c H_p} T^2\left[1 - \left(\frac{T_o}{T}\right)^{1/2}\right]^3\left[1 + \frac{1}{3}\left(\frac{T_o}{T}\right)^{1/2}\right](4). \quad \text{(B6)}$$

APPENDIX C

Interpretation of the optical density (OD) of red cell suspensions utilized the analysis of Twersky, 1970 *a*, *b* and Duysen, 1956.

$$OD_{tot} = OD_{abs} + OD_{sct}, \quad \text{(C1)}$$

where OD_{abs} was the optical density due to absorbance and OD_{sct} the optical density due to light scatter by the cells. OD_{sct} was given by Twersky as

$$OD_{sct} = -\log_{10}\{10^{-ad(Hct - Hct^2)} + q[1 - 10^{-ad(Hct - Hct^2)}]\}, \quad \text{(C2)}$$

where a was the scattering coefficient, d the path length, Hct the hematocrit, and q the fraction of scattered light flux detected by the photosensor. OD_{abs} was different in a particle suspension relative to a solution due to the sieve effect (Latimer and Eubanks, 1962) and was

given by Duysens as

$$OD_{abs} = -m \log_{10} [1 - Hct(1 - t_p)], \qquad (C3)$$

where t_p was the fraction of incident light transmitted through a single particle, and m the number of layers of particles. Note that OD_{abs} was linear with the path width. The linearity of OD_{abs} with path width for red cell suspensions has been experimentally confirmed (Andersen and Sekeli, 1967). OD_{sct} was evaluated using Eq. C2. Values of q and a were obtained from Lipowsky et al., 1980, and, as in their analysis, were assumed constant. The scatter coefficient a and q show little variation for path length >50 μm. In these studies red cell suspensions were allowed to sediment to their equilibrium hematocrit (70–80%). OD_{sct} was calculated for d = 45–200 μm, Hct = 0.7 or 0.8, and a = 0.147 μm^{-1}, q = 0.314. Under these conditions OD_{sct} was nearly constant for d >75 μm (<2% increase between 75 and 200 μm). Between 45 and 75 μm ΔOD_{sct} = 0.058 and $\Delta OD_{sct}/\Delta OD_{tot}$ was 19%. If we removed the OD_{sct} component from the data in Fig. 3 *b* for cell layer heights <80 μm the slope changed from $-1.8\ 10^{-5}$ to $+1.7\ 10^{-5}$. The curves for cell layers >90 μm and <80 μm became nearly indistinguishable. These calculations were consistant with the experimental findings of Lipowsky. Variation of OD_{tot} for cell pack thickness >45 μm was almost totally due to OD_{abs}, therefore OD_{tot} was nearly linear with cell pack height.

Received for publication 16 October 1985 and in final form 22 April 1987.

REFERENCES

Anderson, N. M., and P. Sekelj. 1967. Light-absorbing and scattering properties of nonhaemolysed blood. *Phys. Med. Biol.* 12:173–184.

Brooks, D. E., J. W. Goodwin, and G. V. F. Seaman. 1970. Interactions among erythrocytes under shear. *J. Appl. Physiol.* 28:172–177.

Casson, N. 1959. A flow equation for pigment oil suspensions of the printing ink type. *In* Rheology of Disperse Systems. C. C. Mill, editor. Pergamon Press, New York. 84–104.

Chien, S. 1975. Biophysical behavior of red cells in suspensions. *In* The Blood Cell. 2nd ed. D. Mac N. Surgenor, editor. Academic Press, New York. 1031–1133.

Chien, S., G. King, R. Skalak, S. Usami, and A. L. Copley. 1975. Viscoelastic properties of human blood and red cell suspensions. *Biorheology.* 12:341–346.

Chien, S., L. A. Sung, S. Kim, A. M. Burke, and S. Usami. 1977. Determination of aggregation force in rouleaux by fluid mechanical technique. *Microvasc. Res.* 13:327–333.

Chien, S., S. Usami, H. M. Taylor, J. L. Lundberg, and M. I. Gregersen. 1966. Effects of hematocrit and plasma proteins on human blood rheology at low shear rates. *J. Appl. Physiol.* 21:81–87.

Cokelet, G. R. 1979. The rheology of human blood. *In* Biomechanics. Y. S. Fung, N. Perrone, and N. Anliker, editors. *Proceedings of the Symposium on Biomechanics.* Prentice Hall, La Jolla, CA. 63–104.

Cokelet, G. R., and H. J. Meiselman. 1968. Rheological comparison of hemoglobin solutions and erythrocyte suspensions. *Science (Wash. DC).* 162:275–277.

Copley, A. L., C. R. Huang, and R. G. King. 1973. Rheogoniometric studies of whole human blood at shear rates from 1,000–0.0009 sec^{-1}. Part I. Experimental findings. *Biorheology.* 10:17–22.

Dormandy, J. A., and H. L. Reid. 1978. Controlled defibrination in the treatment of peripheral vascular disease. *Angiology.* 29:80–88.

Drasler, W. J. 1984. Viscoelastic properties of the normal and sickled erythrocyte membrane. Ph.D. thesis, University of Minnesota, Minneapolis, MN. 100–103.

Duysens, L. N. M. 1956. The flattening of the absorption spectrum of suspensions, as compared to that of solutions. *Biochim. Biophys. Acta.* 19:1–12.

Fahraeus, R. 1929. The suspension stability of blood. *Physiol. Rev.* 9:241–274.

Fung, Y. C. 1984. Biomechanics: Mechanical Properties of Living Tissues. Springer-Verlag, New York. 26–27, 76–77.

Huang, C. R., R. G. King, and A. L. Copley. 1973. Rheogoniometric studies of whole human blood at shear rates down to 0.0009 sec^{-1}. Part II. Mathematical interpretation. *Biorheology.* 10:23–28.

Humphreys, W. V., A. Walker, and E. Charlesworth. 1976. Altered viscosity and yield stress in patients with abdominal malignancy: relationship to deep vein thrombosis. *Br. J. of Surg.* 63:559–561.

Latimer, P., and A. H. Eubanks. 1962. Absorption spectrophotometry of turbid suspensions: a method of correction for large systematic distortions. *Arch. Biochem. Biophys.* 98:274–285.

Lipowsky, H. H., S. Usami, S. Chien, and R. N. Pittman. 1980. Hematocrit determination in small bore tubes from optical density measurements under white light illumination. *Microvasc. Res.* 20:51–70.

Meiselman, H. J. 1980. Measures of blood rheology and erythrocyte mechanics. *In* Erythrocyte Mechanics and Blood Flow. Alan R. Liss, Inc., New York. 75–117.

Meiselman, J. J., and E. W. Merrill. 1967. Hemorheology, hemodilution and the effect of low molecular weight dextran. *Bibl. Anat.* 9:288–295.

Merrill, E. W. 1969. Rheology of blood. *Physiol. Rev.* 49:863–888.

Merrill, E. W., and G. A. Pelletier. 1967. Viscosity of human blood: transition from Newtonian to non-Newtonian. *J. Appl. Physiol.* 23:178–182.

Merrill, E. W., C. S. Cheng, and G. A. Pelletier. 1969. Yield stress of normal human blood as a function of endogenous fibrinogen. *J. Appl. Physiol.* 26:1–4.

Merrill, E. W., A. M. Benis, E. R. Gilliland, T. K. Sherwood, and E. W. Salzman. 1965. Pressure flow relations of human blood in hollow fibers at low flow rates. *J. Appl. Physiol.* 20:954–967.

Merrill, E. W., E. R. Gilliland, G. Cokelet, H. Shin, A. Britten, and R. E. Wells, Jr. 1963. Rheology of human blood near and at zero flow. *Biophys. J.* 3:199–213.

Radtke, H., R. Schneider, R. Witt, H. Kiesewetter, and H. Schmid-Schoenbein. 1984. A measuring device to determine a universal parameter for the flow characteristics of blood: measurement of yield stress in a branched capillary. *Adv. Exp. Med. Biol.* 169:851–857.

Thurston, G. B. 1972. Viscoelasticity of human blood. *Biophys. J.* 12:1205–1217.

Thurston, G. B. 1973. Frequency and shear rate dependence of viscoelasticity of human blood. *Biorheology.* 10:375–381.

Thurston, G. B. 1978. Effects of hematocrit on blood viscoelasticity and in establishing normal values. *Biorheology.* 15:239–249.

Twersky, V. 1970*a*. Interface effects in multiple scattering by large, low refracting, absorbing particles. *J. Opt. Soc. Am.* 60:908–914.

Twersky, V. 1970*b*. Absorption and multiple scattering by biological suspensions. *J. Opt. Soc. Am.* 60:1084–1093.

Van Assendelft, O. W. 1970. Spectrophotometry of Haemoglobin Derivatives. Van Gorcum, Thomas, Assen, Netherlands.

Weisberg, S. 1980. Applied Linear Regression. John Wiley & Sons, Inc., New York. 47–50.

Whelan, J. A., C. R. Huang, and A. L. Copley. 1971. Concentration profiles in erythrocyte sedimentation in human whole blood. *Biorheology.* 7:205–212.